Development of a Smart Dual-Energy Crop Dryer with Heat Recovery Integration: Zero-Load Thermal Dynamics Test Validation

N.C. Ezeanya[1], N.R. Nwakuba[1*], P.C. Obumseli[1], C.C. Egwuonwu[1], G.I. Nwandikom[1], S.O. Alagbaoso[2], N.E. Njoku[2]

[1]Department of Agricultural and Biosystems Engineering, Federal University of Technology, Owerri, Nigeria.
[2]Department of Food Science and Technology, Federal University of Technology, Owerri, Nigeria.

ABSTRACT: Innovative drying strategies are essential to the advancement of sustainable postharvest processing. This work presents the development and zero-load thermal characterization test of a smart dual-energy crop dryer integrated with a heat recovery unit. To improve thermal stability and energy efficiency, the dryer incorporates an Arduino-based control unit, solar and electric heating, and heat recovery. According to test data, the solar collector maintained a 38 to 45% thermal gain over ambient conditions and a 40.9% temperature increase in the drying air while reaching temperatures of up to 65°C. It exhibited a remarkable thermal efficiency of 80.76%. The dryer adaptively consumed 74.1% electric and 25.9% solar energy, guaranteeing a steady heat supply during variable solar radiation. A heat-up time of 6.2 to 12 minutes was recorded, with the best performance occurring between 55 °C and 60°C and 1.5 m/s and 2.0 m/s of air velocity. The dryer's heat-up behaviours were successfully predicted by a fitted quadratic model (R^2 = 0.9585). The exhaust heat recovery system reduced energy loss and improved the moisture extraction effectiveness by providing low-humidity preheated air. These results demonstrate the dryer's fast response time, energy flexibility, and appropriateness for off-grid crop drying.

KEYWORDS: Hybrid solar dryer, heat-up time, thermal efficiency, photovoltaic energy, energy analysis.

[Received Jul. 13, 2025; Revised Sep. 10, 2025; Accepted Sep. 27, 2025] Print ISSN: 0189-9546 | Online ISSN: 2437-2110

I. INTRODUCTION

The agrifood sector continues to face postharvest losses, especially in sub-Saharan Africa, where insufficient technologies for drying and preservation cause approximately 30% of harvested crops to be lost (FAO, 2022). In food crop preservation, drying is one of the most crucial and energy-consuming processes. Conventional sun drying, even though it is commonly utilized, faces many limitations, such as large space requirements, susceptibility to contamination and quality depletion, being heavily reliant on the weather, and having irregular drying rates (Nwakuba *et al,* 2020; Afzal *et al*, 2023). A better scientific approach was adopted to harness the inexhaustible and non-polluting energy of the sun for crop drying through the adoption of solar dryers, which are mainly in the form of integral, distributed, and mixed-mode designs (Hani *et al*, 2022). Despite their contrasting features and operational modes, they have a common shortfall, which is the derivation of energy from a time- and location-dependent source (solar irradiance). Others include low energy efficiency (≤ 30%) due to poor heat transfer between the airstream and food products and considerable chimney thermal loss (Beigi, 2016; Nwakuba *et al,* 2018). These constraints have led to the development of dual-energy drying systems, which incorporate supplemental power sources like biomass burners or electrically powered heaters. However, the use of solar thermal technology in agricultural processes in Nigeria has recently become more prevalent as an energy-saving and environmentally friendly strategy. Compared to other renewable energy sources like wind and shale, it is considered preferable due to its abundance, green nature, inexhaustibility, increased cost of fuel, and public power supply (Nwakuba *et al,* 2017a; Zoungrana and Çakmakci, 2021). By maintaining thermal stability during times of low solar irradiation, these hybrid arrangements improve drying dependability. But energy usage is still an issue, especially when drying is dominated by auxiliary sources. Additionally, a considerable quantity of heat is lost through exhaust air, which lowers the optimal energy utilization.

Various published works have recently centred on the advancement of dual-energy-source drying systems. For example, Chauhan and Kumar (2021) developed a hybrid solar-biomass dryer that showed better drying time than solar-only systems when applied for turmeric drying. However, their design had no incorporation of a waste heat recovery system and lacked thermal automation. Also, Oliveira *et al* (2022) developed a hybrid solar-electric dryer for drying vegetables and fish to sustain drying temperature under overcast situations. However, their system required considerable amounts of auxiliary energy and was controlled manually. A solar-electric dryer with an Arduino-based control system to modify humidity and temperature was pitched by Babatunde *et*

*Corresponding author: nrnwakuba@gmail.com

doi: http://doi.org/10.63746/njtd.v22i5.3818

al (2023). Although this was an advancement in the direction of automation, the study failed to tackle idle system performance or loss of energy. In their evaluation of heat recovery systems in drying technologies, Kumar and Raj (2022) found that more than 25–30% of input heat is usually lost to the ambience, highlighting the need to collect and recycle waste heat. Afzal *et al* (2023) developed and assessed the performance of a hybrid mixed-mode solar-electric dryer for peach, apple slices, and chilli with a mean thermal efficiency of 33%. A thermal performance evaluation of a solar-electric wood dryer with a heat recovery unit was conducted by Selimenfendigil *et al* (2021), but was fraught with precise parameter control. Other various hybrid solar designs have been reported for different plant-based products drying (Roratto *et al.,* 2020; Shreelavaniya *et al.,* 2021; Mugi *et al.,* 2022), but none had full incorporation of a heat recovery system with smart control of the operational variables, which include measuring, recording, displaying, and storing drying parameters for enhanced system efficiency, product quality, and reduced human involvement.

Despite advancements in food product drying technologies, there are still significant research gaps. The high energy consumption of contemporary dual-energy source dryers is largely due to the lack of energy recycling mechanisms and smart electronic controls. Additionally, there are a few thermal investigation studies conducted under zero load conditions, which are crucial for understanding internal heat distribution and system behaviour. A comprehensive strategy integrating automation, energy efficiency, and hybrid-heat sources is often overlooked in existing designs. This study aims to address these gaps by developing a cost-effective solar crop dryer that integrates a dual-heating system, exhaust heat recovery mechanism, a microprocessor-primed system for real-time operation, and unloaded-state thermal energy characterization. The results will serve as a foundation for smart, energy-resilient, and ecologically friendly drying remedies for subsistence and commercial-scale applications, as well as give insight into the dryer's thermal behaviour under idle state, evaluating its potential for effective drying operations. The present study considers the materials and instrumentation involved in the design and construction processes of the smart dual-source electric dryer, the description and operational protocols of the dryer, as well as zero-load test validation. The results obtained therein involved thermal assessment, energy contribution of the heat sources, heat recovery unit evaluation, and thermal response time and energy consumption analysis at varying input variables. These findings were presented in descriptive, tabular, and graphical forms.

II. MATERIALS AND METHODS

A. Theoretical Analysis: Heat requirement of the SDED

The overall heat energy needed to desorb moisture from a high-moisture content product ($\mathcal{Q}_t$), such as a tomato, was estimated using Eq. (1) (Afzal *et al,* 2023):

$$\mathcal{Q}_t = \mathcal{W}_w . \mathcal{C}_p . dt \quad (1)$$

Where $\mathcal{W}_w$ is the weight of extracted moisture (kg), $\mathcal{C}_p$ is the specific heat capacity of tomato (3.98 kJ/kg/K), and dt is the temperature change in the drying chamber (K).

Quantity of moisture desorbed:

The dryer was designed based on the physico-properties of red tomatoes. The quantity of desorbed moisture during drying is estimated as:

$$\mathcal{Q}_m = \mathcal{C}_b \left(\frac{MC_1 - MC_2}{1 - MC_2}\right) \quad (2)$$

Where $\mathcal{C}_b$ is the batch capacity of the dryer (25 kg), MC_1 and MC_2 are the initial and final moisture contents of the tomato (% w.b), respectively.

The heat requirement for moisture evaporation ($\mathcal{Q}_{ev}$) is given by

$$\mathcal{Q}_{ev} = MC\left(h_g - h_f\right) \quad (3)$$

Where MC is the moisture content of the fresh product (%w.b), h_g and h_f are the vapour and liquid enthalpy phases of water (2583 kJ/kg and 188 kJ/kg), respectively.

Heat generation of the electric coil:

The amount of heat generated by the DC resistance coil ($\mathcal{Q}_c$) is given by (Nwakuba *et al,* 2020):

$$\mathcal{Q}_c = \frac{\mathcal{P}_\mathcal{C}}{A.L} \quad (4)$$

Where $\mathcal{P}_\mathcal{C}$ is the coil power (W), A is the cross-sectional area of the coil (m²), and L is the coil length (m).

Drying air requirement:

The theoretical quantity of air required to transfer heated air into the drying cavity is calculated as (Nwakuba *et al,* 2017b):

$$\mathcal{Q}_a = \frac{\mathcal{Q}_m}{\mathcal{C}_p \rho_a dt} \quad (5)$$

Where ρ_a is the density of air (1.2922 kg/m³).

Estimation of solar air-heater area and absorbed flux:

The area of the solar collector is calculated using the expression (Nwakuba *et al,* 2018b; Nwakuba *et al,* 2020):

$$\mathcal{A}_\mathcal{C} = \frac{\mathcal{Q}_u}{\mathcal{K}_e . \alpha_g . \tau_g . I_s} \quad (6)$$

Where $\mathcal{Q}_u$ is the collector's useful heat (kW), $\mathcal{K}_e$ is the heat extraction coefficient (0.7), denoting the absorbance (α_g = 0.84) and effective transmittance coefficient of glass (τ_g = 0.06), and I_s is the mean instantaneous solar irradiance (852.411 W/m²).

The absorbed solar flux (ϕ_a) in the solar-air heater is given by:

$$\phi_a = \alpha_g . \mathcal{A}_\mathcal{C} . I_s \quad (7)$$

The conventional thermal loss ($\mathcal{Q}_{loss}$) from the air heater is expressed as (Afzal *et al.,* 2023):

$$\mathcal{Q}_{loss} = \frac{dt}{\mathcal{Q}_R} \quad (8)$$

Where the thermal resistance ($\mathcal{Q}_R$) is calculated as:

$$\mathcal{Q}_R = \frac{dx}{\mathcal{A}_\mathcal{C} . k} \quad (9)$$

Where k is the thermal conductivity of the wooden material (W/Km).

It is worth noting that the mean ambient temperature (T_a) = 40.22 °C, and the mean collector outlet temperature (T_o) = 56.67 °C.

∴

$percent$ increase in heat generation of the solar collector, $\%dT = \left(\frac{T_o - T_a}{T_a}\right) * 100 = 40.9\%$

Airflow and duct size:

Air speed (v) = 1.5 m/s, solar collector duct diameter, D = 87 mm = 0.087 m

The cross-sectional area of the duct (A) becomes

$$A = \frac{\pi D^2}{4} = 0.00595\ m^2 \quad (10)$$

Volumetric flow rate of air in the solar collector unit:

$\dot{V} = Av = 0.008925$ m³/s

∴ The mass flow rate of air ($\dot{m}$):

$\dot{m} = \rho\dot{V} = 0.01071$ kg/s

Solar energy contribution:

$$E_s = \kappa \int_0^{t_\hbar} (A_c * I_s) dt \quad (11)$$

$E_s = 0.05 * 0.2572 * 852.411 * 5160\ J$

$E_s = 56563.92$ J (or 56.56 kJ)

Where $\kappa = \alpha_g . \tau_g$, $t_\hbar$ is the total duration of the high solar exposure (5160 s), A_c is the solar collector area = 0.2572 m², dt is the time increment in the integral, and t is the duration of solar heating (5 min).

Solar collector efficiency and thermal energy gain:

Solar collector efficiency (η_{sc}) refers to the ratio of the useful energy (Q_u) to the solar energy input (Q_s), expressed as (Nwakuba et al., 2020):

$$\eta_{sc} = \left(\frac{Q_u}{Q_s}\right) * 100 = \frac{\dot{m} c_p (T_0 - T_a)}{I_s A_c} * 100 \quad (12)$$

$$\therefore \eta_{sc} = \frac{176.06}{219.24} * 100 = 80.76\%$$

Electric energy contribution:

This is calculated using (Nwakuba *et al.,* 2020):

$$E_\mathfrak{h} = \frac{\mathfrak{p}_\mathfrak{h} * t}{60} \quad (13)$$

$E_\mathfrak{h}$ = 45 Wh (162000 J or 162 kJ)

Where $\mathfrak{p}_\mathfrak{h}$ is the heater's power rating (180 W) and t is the mean heater ON time (15 min).

Total energy and percentage contributions:

The overall thermal energy generated by SDHD is the summation of the heat energy of the solar collector and the DC heater (Nwakuba et al., 2020; Hadibi *et al.,* 2023):

$$E_t = \kappa \int_0^{t_\hbar} (A_c * I_s) dt + \mathfrak{p}_\mathfrak{h} * t \quad (14)$$

Computing for 1 hour (i.e., 12 intervals of 5 minutes)

$E_t = E_s + E_\mathfrak{h} = (56.56 + 162)$ kJ = 218.56 kJ.

This indicates that the overall solar energy intake at 5% transmissivity-absorptivity efficiency in an hour is about 56.56 kJ.

B. Materials and Instrumentation for Zero-Load Test Validation

The materials used for the no-load assessment of the smart dual-energy-source crop dryer (SDED) included a handheld digital pyranometer of model SM206-SOLAR, an SD memory card with card reader, a laptop computer, temperature and relative humidity sensors, and other ancillary components, such as a 180-Watt DC electric heater, an Arduino microprocessor used for automation, control, and regulation of air temperature and humidity, a liquid crystal display, a matrix keypad for inputting different air temperatures and operating time values, a DC fan, 2 x 230-Watt polycrystalline solar panels, and a deep-cycle battery with specifications: tubular design, 12 V, 220 Ah, and charge controller. The datasheets provided by the manufacturers provided the specifications for these components (Exide Technologies, 2021; JinkoSolar, 2022; Arduino, 2023).

C. Equipment Development and Description

The equipment used in this research is a smart dual-energy crop dryer with heat recovery integration, developed at the Agricultural and Biosystems Engineering Department of the Federal University of Technology, Owerri. It consists of these components: collector air inlet, centrifugal fan, solar collector unit with glazing cover, chimney, exhaust air centrifugal fan, drying unit, heat recovery unit, frame support, rollers, thermistor sensors, Arduino microprocessor unit (MPU), and charge controller (Figure 1). To lower the costs of equipment development and product drying, locally accessible glazing material (plain glass) was sourced to transfer and capture solar flux in the air heater unit. The inlet axial flow fan was selected based on the airflow required to transfer the generated enthalpy into the drying cavity. The fans and the resistance/heating coil, as well as the electronic devices, were connected to the control unit, which is powered by the deep-cycle accumulator, charged by the photovoltaic cells (solar panels).

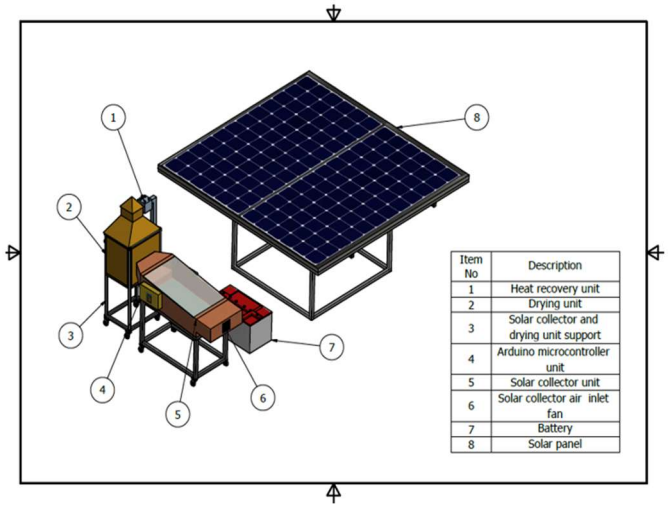

Figure 1: Pictorial view of the SDED.

a. Collector air inlet fan: This is an axial flow DC fan (4 W) mounted at the inlet of the solar collector unit. It works in conjunction with the microprocessor unit to admit ambient air into the dryer at a desired airflow rate.

b. Solar collector unit: It consists of a rectangular-shaped box, the sides of which are made of soft wood. It has dimensions of 703 mm in length, 400 mm in width, and a depth of 190 mm. The top of the collector unit is covered with a 4 mm-thick plain glass, having the same cross-sectional area as the collector surface. The base of the collector unit contains the absorber plate in the form of a rectangular-shaped galvanized sheet plate of 3 mm thickness and painted dull black to enhance thermal heat absorption. The absorber plate overlies the nano-phase change thermal storage unit, which consists of paraffin wax

and titanium oxide. The surface of the solar collector chamber is tilted southward in the northern hemisphere at an angle of 15° to capture optimum solar flux (Tiwari, 2012; Nwakuba *et al.,* 2017b). The value of this angle was derived using Equation (1), expressed as:

$$\beta = 10 + \text{lat}\,\emptyset \quad (15)$$

Where: β = angle of tilt of the solar collector (degrees);
∅ = latitude of collector location, which is FUTO (5.4°N).

The exit of the collector unit tapered slightly and acts as the collector air exit duct as well as the air inlet duct to the drying unit.

c. Drying unit: This is in the form of a stainless-steel box, which has dimensions of 315 mm length, 315 mm width, and 375 mm height. The interior of the drying unit consists of a drying tray where materials to be dried are placed. The tray is a rectangular-shaped rack made of stainless-steel wire mesh and framed with wood. It has dimensions of 264 mm length, 264 mm width, and a height of 43 mm. At the base of the dryer unit is the DC heating coil. The walls of the drying unit were lagged with fiberglass and kaolin of 2 mm thickness to minimize heat loss by conduction.

d. Chimney: Directly above the drying unit is the chimney, which facilitates the removal of moist exhaust air from the drying unit. The chimney has two air exit points; the first point leads to the atmosphere, whereas the second point leads into the exhaust heat recovery unit. At the exit of the chimney is the exhaust air fan, which facilitates moist air removal from the drying unit.

e. Heat recovery unit: This is in the form of a square pipe of cross-sectional area 37 mm x 37 mm, the entrance of which is connected to the second exit point of the chimney, while the exit of the heat recovery unit is connected to the base (second entrance) of the drying unit. In between the entrance and exit points of the recovery unit is the moist air dehumidifying unit, which consists of a metal box of dimensions 90 mm x 90 mm x 95 mm, containing desiccants like silica gel and activated carbon.

f. Frame support: Both the solar collector and the drying units rest on supports made of square pipes. These supports rest on 8 rollers for easy movement of the dryer. The orthographic and exploded views of the developed SDED are shown in Figures 2 and 3.

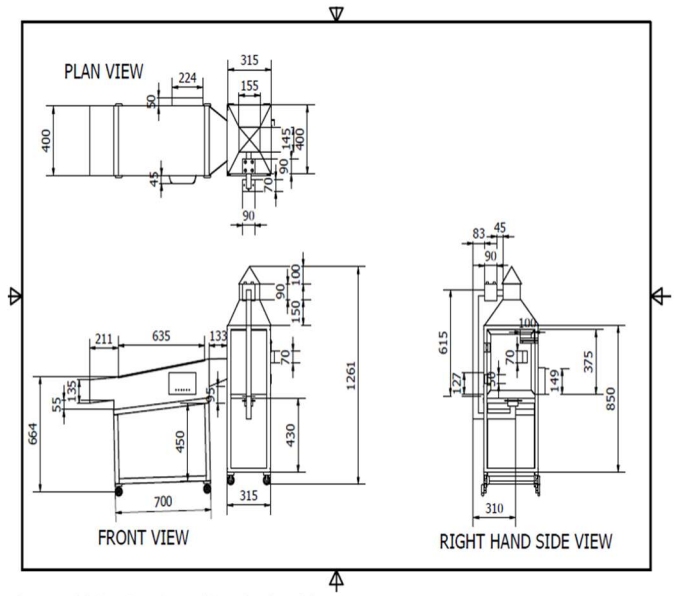

Figure 2: Third-angle orthographic projection of the SDED.

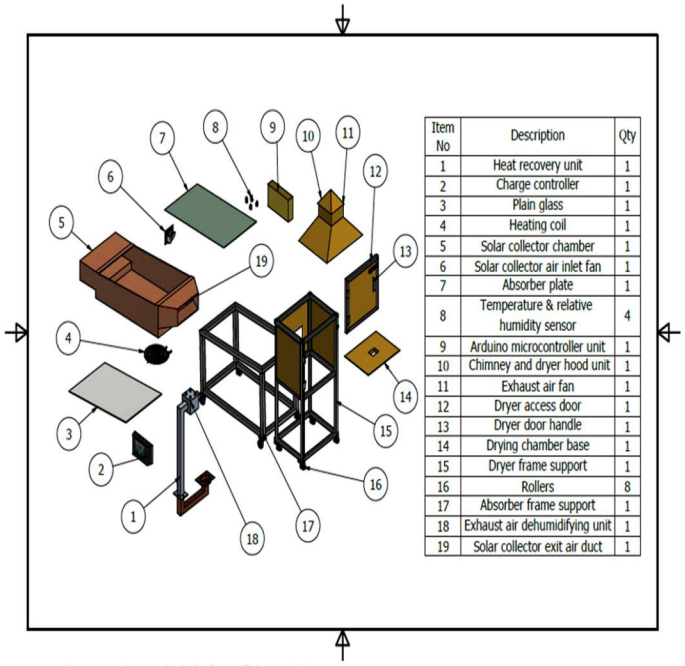

Item No	Description	Qty
1	Heat recovery unit	1
2	Charge controller	1
3	Plain glass	1
4	Heating coil	1
5	Solar collector chamber	1
6	Solar collector air inlet fan	1
7	Absorber plate	1
8	Temperature & relative humidity sensor	4
9	Arduino microcontroller unit	1
10	Chimney and dryer hood unit	1
11	Exhaust air fan	1
12	Dryer access door	1
13	Dryer door handle	1
14	Drying chamber base	1
15	Dryer frame support	1
16	Rollers	8
17	Absorber frame support	1
18	Exhaust air dehumidifying unit	1
19	Solar collector exit air duct	1

Figure 3: The exploded view of the SDED.

D. Mode of Operation

The SDED uses two heat sources, *viz*., solar energy and electricity. Solar energy is harnessed by the solar air heater chamber, while the auxiliary/supplemental heat (electrical energy) is supplied by the heating coil, which is powered by the DC deep-cycle accumulator charged by the solar panels through a charge controller unit. The auxiliary heating unit provides routine application of the hybrid SDED during overcast climatic conditions. The Arduino MPU works to switch between these energy sources so that the dryer can be maintained at a given drying temperature and airflow rate. To operate the hybrid SDED, the microprocessor unit is turned on, the desired temperature and airflow velocity values are input

using the matrix keypad, and the dryer begins to function within the selected operating threshold. Initially, both the solar-air heater (collector chamber) and the heating coil will contribute heat to the drying chamber. Once the temperature of the drying unit exceeds the preset temperature by 2°C, the heater will be automatically disconnected, and the dryer will continue to run only on the heat from the solar collector unit. When the temperature of the drying unit drops below the preset temperature by 2°C, the heater will be automatically reconnected, and the dryer will be powered once again by both solar energy and heat from the heating coil. Therefore, the drying cavity temperature fluctuates between ± 2°C of the preset temperature.

E. Zero-Load Validation of the SDED

In conducting the zero-load validation test, the dryer was set up in an open area free from high-rise structures and trees so as to preclude the impact of shading. All the dryer accessories, including the battery, solar panels, charge controller, and Arduino microprocessor unit, were properly connected. The dryer was aligned in the north-south direction with the face facing south as recommended in literature (Tiwari, 2012). The performance of the dryer was tested at three preset temperatures of 45, 55, and 65°C, at two air velocities of 1.5 and 2.5 m/s. The experiment was scheduled using the Central Composite Design (CCD) method of Design-Expert Statistical Package (ver. 11.1), with a corresponding response variable (Thermal response time) which was subjected to factorial statistical randomization to avoid bias and minimize test errors.

For each test, the SDED was switched on, and the desired temperature and air velocity were keyed into the Arduino MPU to determine the thermal response duration of the drying chamber to attain a steady-state condition. The smart memory card was inserted into a slot in the MPU, and the dryer was allowed to run according to the preset threshold operational conditions. The smart storage medium recorded dryer data every 1 minute for the number of replications required. The data recorded by the smart card were temperature and relative humidity values at the ambient, solar collector unit, drying unit, and chimney points. Each point of data recording was signalled by a beep. The handheld pyranometer was used to measure the insolation that corresponded to each data recording time. After each experiment, the values of the input parameters (temperature, air velocity, and observation time) were reset at the MPU, and the experiment was repeated for other input parameters. After each test, the card was removed and inserted into the laptop computer to harness/compile the data collected by the card. The zero-load validation was done at the Department of Agricultural and Biosystems Engineering of the Federal University of Technology, Owerri (FUTO), between March and May 2025. FUTO is situated at a latitude of 5.3927^0N, and a longitude of 7.02^0E.

IV. RESULTS AND DISCUSSION

A. Collector Thermal Performance Analysis

The performance test of the smart dual-energy-source dryer (SDED) yields pertinent data on heat energy production, temperature and relative humidity profiles, and chamber heat-up (thermal response times), all for the enhancement of prospective designs. A thermal characterization of SDED in the unloaded state is depicted in Figure 4, showing the periodic fluctuations in temperature of the solar collector and ambient air at varying solar radiation intensities. Data were collected on the SDED periodically on exposure to the sunlight between 10:48 am and 4:26 pm. The behaviour of the system makes it evident that it has a strong thermal response and effectively converts solar radiation into thermal energy that could potentially be utilized for drying crops.

During the periods of variable solar exposure, the solar collector temperature continuously surpassed the ambient air temperature during the evaluation. It's noteworthy that the solar collector reached temperatures between $35 \leq T_a \leq 65$°C, and the ambient temperature varied between $30 \leq T_a \leq 43$°C. An ambient temperature of 41°C was measured at 13:16, whereas the collector recorded a high temperature of almost 65°C. This results in a 58% increase in the heat generation capacity of the solar collector (relative to the ambient condition) and high drying air enthalpy, suggesting that the solar collector is a suitable supplementary energy source during periods of variable solar flux. Throughout the entire observation period, the collector consistently raised the mean temperature by 38–45%. This sort of thermal increase is necessary to guarantee efficient drying of a wide range of high-moisture food products requiring consistent heat between 45 and 60°C to absorb moisture safely and effectively. It lowers dependency on supplementary heating systems and boosts thermal efficiency, thus rendering it appropriate for decentralized, off-grid uses in suburban agro-processing. This is especially important in tropical locations where solar energy is plentiful but underused (Nwakuba *et al.,* 2020; Ahmed and Zaman, 2021).

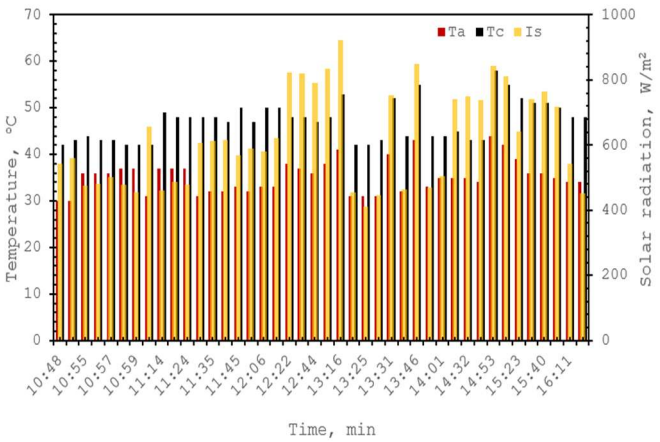

Figure 4: Variation of ambient temperature and solar radiation with time.

Between 12:00 pm and 2:00 pm, the solar flux peaked at around 900 W/m^2, which closely matched the thermal response of the solar collector. This strong correlation between the input solar flux and collector temperature demonstrates the SDED's swift response capacity to solar absorption, reducing thermal lag and boosting productive thermal energy. Crucially, beyond 3:00 pm, when sun intensity began to decrease, the collector

maintained temperatures substantially greater than the ambient air, suggesting strong insulation and heat retention. The smart dryer exhibited exceptional capabilities in terms of thermal gain and solar energy consumption. The dryer surpassed the solar tunnel dryer reported by Bala *et al.* (2020) and accomplished a 20 – 30% collector-to-ambient temperature increase under comparable irradiance contexts. Similar works on flat-plate collectors with temperature variations below 15 °C were reported by Sepehrimehr and Kohan (2015) and Hossain *et al.* (2018), whereas the SDED often demonstrated variations higher than 20°C. This greater thermal response of SDED is primarily attributed to its judicious collector geometry design, improved absorptivity, and insulation, which boost solar radiation collection and minimize thermal losses.

B. Energy input from SDED heat sources

The energy split of the solar collector and DC electric heat contributions during the no-load thermal characterisation of SDED is shown in Figure 5. It indicates that 74.1% of the overall heat input came from DC electric heating, while the solar collector generated 25.9%. This distribution illustrates how SDED's real-time adaptive control mechanism flexibly switched between heat sources during the test due to erratic solar flux. Despite the weather constraints, the solar system performed admirably. With an efficiency of 80.76%, the solar-air heater (collector) demonstrated a high level of efficacy in transforming incident radiation into useful thermal energy. Substantial thermal gain from the collector was confirmed by the 40.9% temperature rise between the inflowing air (40.22°C) and the collector exit air (56.67°C). From the foregoing, the dominant energy portion from the electric heater arose due to overcast weather conditions, intermittent solar flux, and transitional times. The smart dual-energy-source design is validated by the system's capacity to instantly incorporate electric heater supply and harness high-efficiency solar energy (in unstable weather). The thermal evaluation confirms that the heat recovery system and programmable/electronic control unit provide operational flexibility and energy reliability.

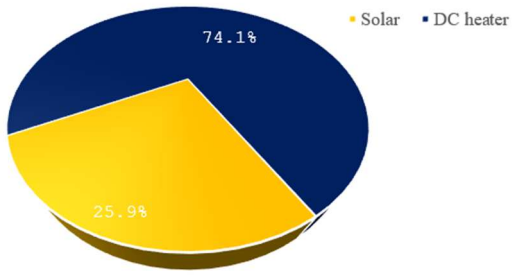

Figure 5: Pie chart illustration of the energy contribution of heat sources.

C. Performance of the Heat Recovery Unit

The psychometric and thermal behaviour of SDED with a heat recovery unit over time is depicted in Figure 6. The temperature of the heat recovery unit (T_r) is continually higher than the drying chamber temperature (T_d), with T_r and T_d having their peak values at78°C and 65°C, respectively. This confirms the contribution of the heat recovery unit to thermal improvement by exhibiting a temperature differential of around 20% over the drying chamber temperature. The inflow air preheating potential of the heat recovery unit, which lowers the heat demand on the DC heating source, is proof of its efficacy. This thermodynamic benefit is consistent with research by Adedeji *et al.* (2023), which showed that dryers incorporated with recycling mechanisms potentially boost thermal efficiency by up to 25%. Although the microprocessor controlled the preset chamber temperature, the recirculated heat played a major role in maintaining the temperature threshold. The thermal efficiency of the SDED was confirmed by the incorporation of the recovery unit, which resulted in noticeable decreases in heat-up time and DC electric energy consumption. This not only optimizes resources but also supports environmentally friendly drying methods by reusing thermal energy that would otherwise be lost. The effectiveness of the recovery unit is further supported by fluctuations in relative humidity. The relative humidity of the drying chamber (R_d) gradually drops from 70% to 20%, whereas the relative humidity of the recovery unit (R_r) remains below 50% following initial stabilization.

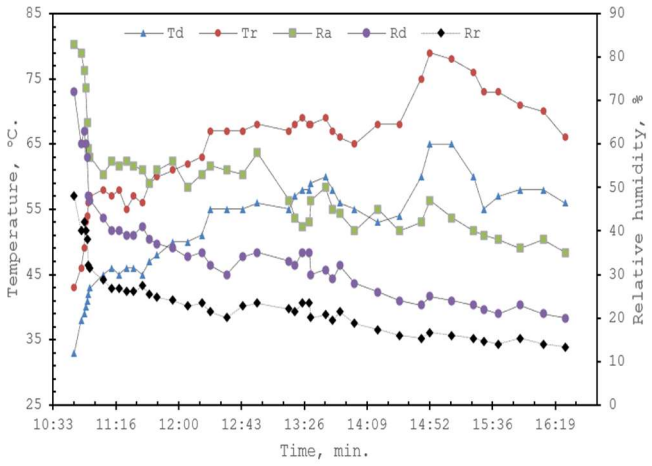

Figure 6: Variation of temperature and relative humidity of the drying chamber and heat recovery unit with time.

As $R_r < R_d < R_a$, this trend suggests that the recycled air is much drier and therefore has greater moisture absorption capacity for subsequent drying. It further implies that, in addition to recycling thermal energy, the heat recovery unit also supplies low-humidity, preheated air, which speeds up the system's moisture removal rate. The steady drop in R_d results in a sustained increase in vapour pressure imbalance between the drying chamber and the ambient air, which accelerates moisture evaporation. The lower R_r is particularly beneficial for drying efficiency. As a result, less extra energy is required and thermal efficiency is increased. However, the relatively high ambient relative humidity (R_a) confirms the beneficial effect of shielding dryer air from external variations.

According to recent studies, greater T_d and reduced internal relative humidity, maintained by T_r, maximize heat and mass transfer rates, thereby increasing drying efficiency and minimizing total energy use (Kumar and Karthick, 2024; Ndukwu *et al.,* 2023). In line with sustainability objectives, this incorporated temperature and humidity control unit enhances performance.

D. Thermal Response (Heat-up) Time and Energy Consumption Dynamics

One crucial index that establishes the effectiveness of heat build-up within the drying chamber is the thermal response time (TRT or t_Q) (Sepehrimehr and Kohan, 2014; Nwakuba *et al*., 2017a). It is the time required for a crop drying system to attain a steady-state condition necessary for optimal product drying. It is the length of time taken for the drying chamber to equilibrate with the inflow airstream under specific setup conditions after being switched on. TRT is directly affected by the rate at which energy flows from the heat supply unit to the drying compartment. Heat-up (thermal response) times were determined in this study utilising the smart dual-energy-source crop dryer (SDED) at varying preset chamber temperatures, air speeds, and solar intensities.

E. Impact of Air Temperature

Raising the preset chamber temperature threshold marginally shortens the thermal response period at decreasing air velocities. Nevertheless, the temperature increase has a diminishing effect on improving response time as air velocity increases. At a uniform air velocity of 2 m/s, the thermal response time continually dropped with an increase in the chamber preset temperature. The response time decreased to 8 minutes at 65°C from 7 minutes at 45°C. When the temperatures spike, there is a slight rise from 7 to 8 minutes; nonetheless, this fluctuation is tolerable given ambient disruption and the thermal inertia of the dryer system. Further increases in temperature above 60°C appear to generate some flattening or reversal effect, suggesting thermal saturation. The SDED produces the optimum effective thermal response when operated between 55 and 60°C and 2 and 2.5 m/s, according to the surface plot (Figure 7). At these temperatures, energy generation and heat transfer to the drying air are improved as the dryer rapidly reaches its desired operating temperature. This validates the report of Adeniran *et al*. (2023), which shows that a combination of high airflow and high temperature reduces the dryer lag period.

F. Impact of Air Velocity

As air velocity increases, TRT shortens at lower temperature levels ($45 \leq t \leq 50$°C) because of more effective convective heat transfer. Raising the air velocity at elevated temperatures ($60 \leq t \leq 65$°C) causes a minor increase in the thermal response period; this might be because of thermal instability, border layer shrinking, or an overriding cooling impact that reduces heating efficiency. The surface's curvature indicates that temperature and air velocity interact nonlinearly. It is worth noting that each temperature level showed a reduction in t_Q as air velocity increased at steady preset chamber temperatures. The response period dropped from 8.5 minutes at 1.5 m/s to 6.2 minutes at 2.5 m/s at 45°C. The t_Q value shortened from 9.5 minutes at 1.5 m/s to 6.8 minutes at 2.5 m/s at 65°C. This behaviour is explained by more rapid heat distribution across the chamber due to improved convective heat transfer at greater velocity. Heat is delivered more swiftly from the heating units through the air stream and lowers the thermal barrier layer surrounding the chamber plenum and tray surfaces.

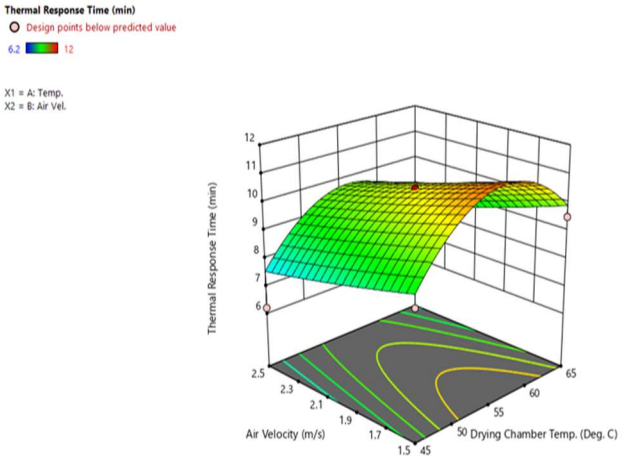

(a)

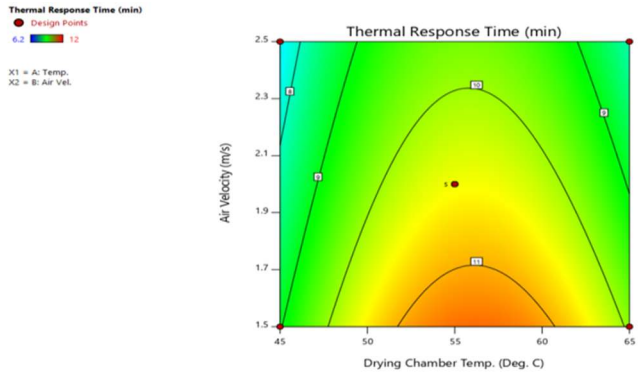

(b)

Figure 7: Response surface and contour plots of the impact of drying chamber preset temperature and air speed on heat start-up time in SDED.

G. Interaction Effect of Process Variables

Table 1's analysis of variance (ANOVA) demonstrates that the established quadratic function was statistically significant ($F = 6.00$, $p = 0.0180$), suggesting that the model well describes the variability of the thermal response of the dryer system. Among the linear parameters, drying temperature ($F = 4.83$, $p = 0.0215$) had a less noticeable impact than drying air velocity ($F = 3.25$, $p = 0.0179$). The temperature quadratic term (t^2) was very significant ($F = 23.63$, $p = 0.0018$), indicating considerable curvature effects. The air velocity quadratic effect (v^2) contributed less, although it was still significant ($p = 0.0098$). There was no statistically

significant interaction between t and v (p = 0.015). The model was found to be adequate for prediction when the lack-of-fit test was non-significant in relation to pure error. In general, the findings show that the response variable under investigation is significantly influenced by both temperature and air velocity, especially when they are expressed in quadratic form.

Table 1: Analysis of variance of the thermal response of SDED at varying temperatures and air velocities.

Source	Sum of Squares	Df	Mean Square	F-Value	P-Value	Significance
Model	33.14	5	6.63	6.00	0.0180	**
t-Temp.	1.14	1	1.14	4.83	0.0215	*
v-Air Vel.	5.14	1	5.14	3.25	0.0179	**
tv	0.0400	1	0.0400	0.0362	0.015	**
t^2	26.11	1	26.11	23.63	0.0018	**
v^2	0.0272	1	0.0272	0.0246	0.0098	**
Residual	7.74	7	1.11			
Lack of Fit	7.74	3	2.58			
Pure Error	0.0000	4	0.0000			
Cor. Total	40.87	12				

* = significant; ** = Highly significant @ P < 0.05

The combined impact of the preset drying chamber temperatures and air velocities on the SDED's TRT is depicted in the 3D surface plot (Figure 7). With a high coefficient of determination ($R^2 > 0.95$), the model, which was developed using Design-Expert® software, demonstrated a high level of predictive accuracy. This establishes a robust relationship between the experimental and predicted values, validating that the model accounts for over 95% of the variability in thermal response duration. The relevance of both linear, interaction, and quadratic factors in capturing system behaviour under the evaluated operational conditions is justified by this high R^2 value, which statistically shows the quadratic model's sufficiency (Montgomery, 2020). In terms of actual parameters, the fitted quadratic regression model is expressed as:

$$t_Q = 10.5 + 0.377t - 0.802v - 0.1tv - 1.94t^2 + 0.063v^2 \quad [R^2 = 0.9585] \qquad (16)$$

Where t_Q, T, and V are the thermal response time (min), drying chamber temperature (°C), and air velocity (m/s), respectively. The positive coefficient of t (0.377) in Eq. (16) indicates that a minor rise in drying chamber temperature lengthens TRT; however, this is mitigated by the substantial negative quadratic term ($-1.94t^2$), which signifies a diminishing return or eventual reduction in t_Q value at elevated chamber temperatures. However, air velocity (v) shows an antagonistic linear impact (-0.802), indicating that the TRT decreases as airspeed increases. When t and v variables increase concurrently, a slight but evident synergistic impact is demonstrated in the relatively small interaction term ($-0.1tv$). The thermal response period of the SDHD was obtained in the range of $6.2 \leq t_Q \leq 12$ minutes at the studied process variables. The optimal t_Q ($6.2 \leq t_Q \leq 7$ min, blue region) was produced at low chamber temperatures and moderate air speeds. The reddish-yellow region response durations are longest at mid-temperatures with low air speed or at high temperatures with extremely high air velocity ($\sim 11 \leq t_Q \leq 12$ min). A similar study involving a solar electric-assisted hybrid crop-dryer was reported by Nwakuba *et al.* (2017a) in which the heat-up times were 57.6 and 51.4 minutes for the solar and hybrid modes, respectively. In contrast, according to comparable research, thermal response durations for conventional solar dryers without electrical support exceeded 15 minutes under identical operational conditions (Mekonnen *et al.,* 2020; Afolabi and Ajayi, 2022).

A further illustration of SDED's thermal behaviour is provided by the colour bands integrated into the 3D surface plot. The colour spectrum of the plot offers a clear visual indication of performance regions. These bands of colour (Table 2) demonstrate that operating in the blue-green domains (6.2 - 10 minutes) promotes increased thermal efficiency, which is essential for off-grid or renewable energy-powered systems that have energy-sensitive crop drying applications. The yellow and red domains (10 – 12 minutes), on the other hand, draw attention to a variable mix that leads to a slow thermal ramp-up, which needs to be circumvented in optimal control conditions.

Table 2: Characterization of colour gradients for thermal response duration in SDED at different drying chamber temperatures and air speeds.

Colour Band/Time Range (min)	Thermal Response Duration (min)	Inference/implication
Blue: $6.2 \leq t_Q \leq 7$	Shortest heat-up durations	Superior heat transfer and maximum thermal yield.
Green: $8 \leq t_Q \leq 9.5$	Moderate heat-up durations	Good thermal performance with efficient heat transfer.
Yellow: $10 \leq t_Q \leq 11$	Slower heat-up durations	Inadequate; moderate energy shortfall
Red: $11.5 \leq t_Q \leq 12$	Longest heat-up durations	A region with excessive energy use, inefficient heat transfer, and considerable start-up energy demand.

H. Energy Insights

The energy consumption of the SDED has an intricate relationship with TRT, which depends on the operational variables (t and v). According to Eq. (16), convective heat transfer is improved by raising air velocity, which shortens the time required to achieve a steady-state condition. Conversely, due to the heightened heat demand, higher preset temperatures initially lead to an increased TRT. However, this increases until a saturation point is reached, at which point energy consumption becomes more efficient, as reflected in the negative quadratic term ($-1.94t^2$). This is corroborated by the 3D surface plot, which indicates that SDED achieved the desired thermal thresholds more quickly at midrange temperature settings ($55 \leq t \leq 60$°C) and moderate air speeds ($1.5 \leq v \leq 2.0$ m/s), resulting in optimal savings in energy

usage. These results are consistent with previously published studies on smart crop drying systems that demonstrated a co-dependence between energy dynamics and temperature response (Ebadi *et al.*, 2021; Jha and Tripathy, 2024). The SDED demonstrated an 80.76% thermal collector efficiency and a 40.9% increase in heat output due to improved heat recirculation compared to its baseline design. The minimum t_Q values (6.2 to 7.5 min) evidenced in the blue-green spectrum of the 3D response plot provide proof of optimal energy consumption and more effective heat accumulation and transfer. This leads to reduced start-up energy requirements and enhanced heat utilization efficiency. This efficiency is essential in off-grid or solar-assisted applications, where energy savings are crucial. However, a more rapid heat response suggests that drying equilibrium will be reached more quickly, which will cut down on idle heating times while maximizing energy efficiency during batch or cycle operation. As the photovoltaic system supplements solar heat in a manner that prevents thermal lag during low irradiance or early starting periods, this efficiency improvement gets increasingly apparent in hybrid mode.

V. CONCLUSION

The design, construction, and performance test of a dual-source solar crop dryer was undertaken under the warm-humid Owerri climatic conditions. The incorporation of a heat recovery unit and an electronic control system substantially boosted the overall dryer's performance by supplying preheated, low-humidity air that would enhance moisture extraction rates and minimize energy loss. Interestingly, under fluctuating solar radiation, the electric source provided 74.1% of the energy, enabling the system to flexibly transition between solar and DC electric heating, guaranteeing thermal continuity during transitory weather.

The thermal response time analysis indicated that optimum performance was achieved at temperatures between 55 and 60°C and air speeds of 1.5 to 2.0 m/s. The rapid heat-up time varied from 6.2 to 12 minutes, depending on the drying chamber temperature and air velocity. The thermal response time was accurately predicted by a quadratic model (R^2 = 0.9585), influenced by the linear and interaction effects of the process variables, demonstrating the efficiency of the smart operational control in minimizing energy consumption and heat-up time.

In general, the SDED design provides a short-lag, energy-efficient operational remedy, particularly in situations where energy savings, sustainability, and dependability are crucial. These outcomes offer fundamental knowledge for future development and expansion of hybrid drying systems designed for agro-processing in regions with limited resources.

AUTHOR CONTRIBUTIONS

N. C. Ezeanya: Writing of original draft, design of the dryer framework, mechanical construction, and technical supervision. **N. R. Nwakuba:** Conceptualization, dryer design and construction, data analysis, final manuscript editing, and correspondence. **P. C. Obumseli:** Literature review and data collation. **C. C. Egwuonwu:** Experimental setup coordination, writing—review & editing. **G. I. Nwandikom:** Literature review, materials sourcing, and graphical illustrations. **S. O. Alagbaso:** Statistical validation, results interpretation, and manuscript proofreading. **N. E. Njoku:** Software programming support, data visualization, and referencing.

ACKNOWLEDGMENTS

The authors acknowledge with gratitude the financial support given by the Tertiary Education Trust Fund (TETFund), under the National Research Fund (NRF) intervention. The assistance rendered by the Federal University of Technology, Owerri, for the award of this research grant (TETFES//DR&D-CE/NRF-2023/SETI/AFS/00391/VOL.1) and its successful accomplishment is sincerely appreciated.

REFERENCES

Adedeji, A. A.; D. A. Aremu and A. S. Ogunlowo (2023). Heat recovery systems in drying technologies: A review of principles and applications. Renewable Energy, 211, 553–565. https://doi.org/10.1016/j.renene.2023.05.017

Adeniran, J. A.; W. I. Okonkwo; D. Aremu and J. T. Oladeji (2023). Energy optimization of hybrid dryers using thermal response and collector efficiency models. Renewable Energy Systems Journal, 45(3), 241–255.

Afolabi, T. J. and B. O. Ajayi (2022). Development and evaluation of a mixed-mode solar dryer with improved thermal energy storage. Solar Energy, 245, 542–550.

Afzal, A.; T. Iqbal; K. Ikram; M. N. Anjum and M. Umair (2023). Development of a hybrid mixed-mode solar dryer for product drying. Heliyon, 9(2023), e14144.

Ahmed, T. and T. Zaman (2021). Modification and performance enhancement of the solar biomass dryer. arXiv. https://doi.org/10.34257/GJREAVOL21IS2PG31

Arduino (2023). Arduino Uno Rev3 technical specifications. Retrieved September 12, 2025, from https://docs.arduino.cc/hardware/uno-rev3

Babatunde, A. A.; L. A. O. Ogunjimi and A. A. Obafemi (2023). Modeling the performance of a smart solar-electric dryer for agricultural produce. Energy Reports, 9, 789–799. https://doi.org/10.1016/j.egyr.2023.02.015

Beigi, M. (2016). Energy efficiency and moisture diffusivity of apple slices during convective drying. Food Science and Technology, 36(1),145-150.

Chauhan, P. S. and A. Kumar (2021). Performance evaluation of a hybrid solar–biomass dryer for turmeric drying. Solar Energy, 224, 1–10. https://doi.org/10.1016/j.solener.2021.06.025

Ebadi, H.; D. Zare; M. Ahmadi and G. Chen (2021). Performance of a hybrid compound parabolic concentrator solar dryer for tomato slices drying. Solar Energy, 215, 44–63.

Exide Technologies (2021). 12V 100Ah deep cycle battery specifications. Exide Batteries. Retrieved September 12, 2025, from https://www.exide.com

FAO (2022). The State of Food and Agriculture 2022: Leveraging automation for food security. Food and Agriculture Organization of the United Nations.

Hadibi, T.; D. Mennouche; A. Boubekri; S. Chouicha; M. Arıcı; W. Yunfeng; W. Ming and F. Fang-

ling (2023). Drying characteristic, sustainability, and 4E (energy, exergy, and enviro-economic) analysis of dried date fruits using an indirect solar-electric dryer: An experimental investigation. Renewable Energy, 218, 1-17. https://doi.org/10.1016/j.renene.2023.119291

Hani, E. H. B.; M. A. Nazari; M. E. Assad; H. F. Fard and A. Maleki (2022). Solar dryers as a promising drying technology: a comprehensive review. Journal of Thermal Analysis and Calorimetry. https://doi.org/10.1007/s10973-022-11501-6

Hossain, M. Z; M. M. Alam; F. B. Hossain; M. S. Sarker; M. A. Awal and N. Jahan (2018). Performance evaluation of a cabinet solar dryer for drying red pepper in Bangladesh. Journal of Agricultural Engineering XLIX:100–09. https://doi.org/10.4081/jae.2018.774

Jha, A. and P. P. Tripathy (2024). Performance evaluation and finite element modelling of heat, mass, and fluid flow inside a hybrid solar dryer during drying of paddy grains. Frontiers in Food Science & Technology, 4 https://doi.org/10.3389/frfst.2004.1411956

JinkoSolar (2022). Polycrystalline solar panel datasheet (100 W model). Retrieved September 12, 2025, from https://www.jinkosolar.com

Kumar, A. and R. Raj (2022). Heat recovery systems in solar drying: a technical review. Journal of Cleaner Production, 370, 133504. https://doi.org/10.1016/j.jclepro.2022.133504

Kumar, P. and K. Karthick (2024). Energy-efficient hybrid drying systems with thermal recovery. Journal of Cleaner Production, 436, 140963. https://doi.org/10.1016/j.jclepro.2023.140963

Mekonnen, A. T.; G. G. Hailu and M. T. Asfaw (2020). Thermal performance evaluation of a natural convection solar dryer. Renewable Energy, 148, 716–726.

Montgomery, D. C. (2020). Design and Analysis of Experiments (10th ed.). Wiley.

Mugi, V. R. and V. P. Chandramohan (2022). Comparison of drying kinetics, thermal and performance parameters during drying guava slices in natural and forced convection indirect solar dryers. Solar Energy, 234, 319–329. https://doi.org/10.1016/j.solener.2022.02.012

Ndukwu, M. C.; C. Ohakwe and E. Kalu (2023). Development and performance of solar dryers with heat recovery for agricultural applications. Solar Energy, 256, 1123–1135. https://doi.org/10.1016/j.solener.2023.03.039

Nwakuba, N.; C. Chukwuezie; S. Asoegwu and K. Nwaigwe (2017a). No-load performance testing of an Arduino-primed hybrid solar-electric crop dryer. ASABE Meeting Presentation at the 2017 ASABE Annual International Meeting, Spokane, Washington, p. 1-15.

Nwakuba, N. R.; S. N. Asoegwu; K. N. Nwaigwe and O.C. Chukwuezie (2017b). Design and development of a hybrid solar-electric dryer for sliced vegetable crops. Journal of Agricultural Engineering Technology,2,48–64.

Nwakuba, N. R.; O. C. Chukwuezie; G. U. Asonye and S. N. Asoegwu (2018). Energy analysis and optimization of thin-layer drying conditions of okra. Arid Zone Journal of Engineering, Technology & Environment, 14(sp i4), 135 – 154.

Nwakuba, N. R.; M. C. Ndukwu; G. U. Asonye; S. N. Asoegwu and G. I. Nwandikom (2020). Environmental sustainability analysis of a hybrid heat source dryer. Polytechnica, 3, 99 -114. https://doi.org/10.1007/s41050-020-00026-2

Oliveira, M.; A. S. da Silva and V. Marinho (2022). Development of a hybrid solar-electric dryer for fish and vegetable drying. Renewable Energy, 182, 114–125. https://doi.org/10.1016/j.renene.2021.10.095

Roratto, T.; R. Monteiro; B. Carciofi and J. Laurindo (2020). An innovative hybrid solar vacuum dryer to produce high-quality dried fruits and vegetables, LWT, 140, 110777, https://doi.org/10.1016/j.lwt.2020.110777

Selimenfendigil, F.; C. Sirin and H. F. Oztop (2021). Improving the performance of an active greenhouse dryer by integrating a solar absorber north wall coated with graphene nanoplatelet-embedded black paint. Solar Energy, 231, 140–148. https://doi.org/10.1016/j.solener.2021.10.082

Sepehrimehr, B. and A. Kohan (2015). Evaluating a hybrid passive solar-electrical dryer for drying grapes. Advances in Environmental Biology, 9(3), 353-355.

Shreelavaniya, R.; S. Kamaraj; S. Subramanian; R. Pangayarselvi; S. Murali and A. Bharani (2021). Experimental investigations on drying kinetics, modeling and quality analysis of small cardamom (Elettaria cardamomum) dried in solar-biomass hybrid dryer, Solar Energy, 227, 635–644, https://doi.org/10.1016/j solener.2021.09.016

Tiwari, G. N. (2012). Solar Energy: Fundamentals, Design, Modeling and Applications. Narosa Publishing House, PVT Ltd., New Delhi. 9th Edition.

Zhou, J.; J. Zhang and H. Ma (2022). Performance enhancement of hybrid solar-electric dryers via optimized thermal management. Applied Thermal Engineering, 209, 118256.

Zoungrana, A. and M. Çakmakci (2021). From non-renewable energy to renewable energy by harvesting salinity gradient power by reverse electrodialysis: A review. International Journal of Energy Research, 45(3), 3495-522.